Directional couplers with integrated carbon nanotube incandescent light emitters

Randy G. Fechner,[1,2] Felix Pyatkov,[1,3] Svetlana Khasminskaya,[1] Benjamin S. Flavel,[1] Ralph Krupke,[1,3,5] and Wolfram H. P. Pernice[1,4,*]

[1]*Institute of Nanotechnology, Karlsruhe Institute of Technology, Karlsruhe 76021, Germany*
[2]*Institute of Microstructure Technology, Karlsruhe Institute of Technology, Karlsruhe 76021, Germany*
[3]*Department of Materials and Earth Sciences, Technische Universität Darmstadt, Darmstadt 64287, Germany*
[4]*Institute of Physics, University of Münster, Münster 48149, Germany*
[5]*ralph.krupke@kit.edu*
[*]*wolfram.pernice@kit.edu*

Abstract: We combine on-chip single-walled carbon nanotubes (SWNTs) emitters with directional coupling devices as fundamental building blocks for carbon photonic systems. These devices are essential for studying the emission properties of SWNTs in the few photon regime for future applications in on-chip quantum photonics. The combination of SWNTs with on-chip beam splitters herein provides the basis for correlation measurements as necessary for nanoscale source characterization. The employed fabrication methods are fully scalable and thus allow for implementing a multitude of functional and active circuits in a single fabrication run. Our metallic SWNT emitters are broadband and cover both visible and near-infrared wavelengths, thus holding promise for emerging hybrid optoelectronic devices with fast reconfiguration times.

References and links

1. R. Kirchain and L. Kimerling, "A roadmap for nanophotonics," Nat. Photonics **1**(6), 303–305 (2007).
2. M. Paniccia, "Integrating silicon photonics," Nat. Photonics **4**(8), 498–499 (2010).
3. A. J. Shields, "Semiconductor quantum light sources," Nat. Photonics **1**(4), 215–223 (2007).
4. A. W. Schell, G. Kewes, T. Schröder, J. Wolters, T. Aichele, and O. Benson, "A scanning probe-based pick-and-place procedure for assembly of integrated quantum optical hybrid devices," Rev. Sci. Instrum. **82**(7), 073709 (2011).
5. A. Huck, S. Kumar, A. Shakoor, and U. L. Andersen, "Controlled coupling of a single nitrogen-vacancy center to a silver nanowire," Phys. Rev. Lett. **106**(9), 096801 (2011).
6. X. Wang, Z. Cheng, K. Xu, H. K. Tsang, and J.-B. Xu, "High-responsivity graphene/silicon-heterostructure waveguide photodetectors," Nat. Photonics **7**(11), 888–891 (2013).
7. N. Youngblood, Y. Anugrah, R. Ma, S. J. Koester, and M. Li, "Multifunctional graphene optical modulator and photodetector integrated on silicon waveguides," Nano Lett. **14**(5), 2741–2746 (2014).
8. H. A. Pohl, *Dielectrophoresis: The Behavior of Neutral Matter in Nonuniform Electric Fields* (Cambridge University, 1978).
9. E. M. Freer, O. Grachev, X. Duan, S. Martin, and D. P. Stumbo, "High-yield self-limiting single-nanowire assembly with dielectrophoresis," Nat. Nanotechnol. **5**(7), 525–530 (2010).
10. R. Krupke, F. Hennrich, H. B. Weber, M. M. Kappes, and H. Löhneysen, "Simultaneous deposition of metallic bundles of single-walled carbon nanotubes using ac-dielectrophoresis," Nano Lett. **3**, 1019–1023 (2003).
11. J. Lefebvre, J. M. Fraser, P. Finnie, and Y. Homma, "Photoluminescence from an individual single-walled carbon nanotube," Phys. Rev. B **69**(7), 075403 (2004).
12. J. A. Misewich, R. Martel, P. Avouris, J. C. Tsang, S. Heinze, and J. Tersoff, "Electrically induced optical emission from a carbon nanotube FET," Science **300**(5620), 783–786 (2003).
13. M. H. P. Pfeiffer, N. Stürzl, C. W. Marquardt, M. Engel, S. Dehm, F. Hennrich, M. M. Kappes, U. Lemmer, and R. Krupke, "Electroluminescence from chirality-sorted (9,7)-semiconducting carbon nanotube devices," Opt. Express **19**(S6 Suppl 6), A1184–A1189 (2011).

Corrected: 25 January 2016

14. D. Mann, Y. K. Kato, A. Kinkhabwala, E. Pop, J. Cao, X. Wang, L. Zhang, Q. Wang, J. Guo, and H. Dai, "Electrically driven thermal light emission from individual single-walled carbon nanotubes," Nat. Nanotechnol. **2**(1), 33–38 (2007).
15. T. Mueller, M. Kinoshita, M. Steiner, V. Perebeinos, A. A. Bol, D. B. Farmer, and P. Avouris, "Efficient narrow-band light emission from a single carbon nanotube p-n diode," Nat. Nanotechnol. **5**(1), 27–31 (2010).
16. A. Högele, C. Galland, M. Winger, and A. Imamoğlu, "Photon antibunching in the photoluminescence spectra of a single carbon nanotube," Phys. Rev. Lett. **100**(21), 217401 (2008).
17. E. Gaufrès, N. Izard, A. Noury, X. Le Roux, G. Rasigade, A. Beck, and L. Vivien, "Light emission in silicon from carbon nanotubes," ACS Nano **6**(5), 3813–3819 (2012).
18. S. Khasminskaya, F. Pyatkov, B. S. Flavel, W. H. P. Pernice, and R. Krupke, "Waveguide-integrated light-emitting carbon nanotubes," Adv. Mater. **26**(21), 3465–3472 (2014).
19. R. Watahiki, T. Shimada, P. Zhao, S. Chiashi, S. Iwamoto, Y. Arakawa, S. Maruyama, and Y. K. Kato, "Enhancement of carbon nanotube photoluminescence by photonic crystal nanocavities," Appl. Phys. Lett. **101**(14), 141124 (2012).
20. R. Miura, S. Imamura, R. Ohta, A. Ishii, X. Liu, T. Shimada, S. Iwamoto, Y. Arakawa, and Y. K. Kato, "Ultralow mode-volume photonic crystal nanobeam cavities for high-efficiency coupling to individual carbon nanotube emitters," Nat. Commun. **5**, 5580 (2014).
21. S. Imamura, R. Watahiki, R. Miura, T. Shimada, and Y. K. Kato, "Optical control of individual carbon nanotube light emitters by spectral double resonance in silicon microdisk resonators," Appl. Phys. Lett. **102**(16), 161102 (2013).
22. A. Noury, X. L. Roux, L. Vivien, and N. Izard, "Enhanced light emission from carbon nanotubes integrated in silicon micro-resonator," Nanotechnology **26**(34), 345201 (2015).
23. J.-M. Liu, *Photonic Devices* (Cambridge University, 2009).
24. A. Yarif, *Optical Electronics in Modern Communications* (Cambridge University, 1997).
25. D. Taillaert, W. Bogaerts, P. Bienstman, T. F. Krauss, P. Van Daele, I. Moerman, S. Verstuyft, K. De Mesel, and R. Baets, "An out-of-plane grating coupler for efficient butt-coupling between compact planar waveguides and single-mode fibers," IEEE J. Quantum Electron. **38**(7), 949–955 (2002).
26. K. Moshammer, F. Hennrich, and M. M. Kappes, "Selective suspension in aqueous sodium dodecyl sulfate according to electronic structure type allows simple separation of metallic from semiconducting single-walled carbon nanotubes," Nano Res. **2**(8), 599 (2009).
27. B. S. Flavel, M. M. Kappes, R. Krupke, and F. Hennrich, "Separation of single-walled carbon nanotubes by 1-dodecanol-mediated size-exclusion chromatography," ACS Nano **7**(4), 3557–3564 (2013).
28. B. S. Flavel, K. E. Moore, M. Pfohl, M. M. Kappes, and F. Hennrich, "Separation of single-walled carbon nanotubes with a gel permeation chromatography system," ACS Nano **8**(2), 1817–1826 (2014).
29. A. Vijayaraghavan, F. Hennrich, N. Stürzl, M. Engel, M. Ganzhorn, M. Oron-Carl, C. W. Marquardt, S. Dehm, S. Lebedkin, M. M. Kappes, and R. Krupke, "Toward single-chirality carbon nanotube device arrays," ACS Nano **4**(5), 2748–2754 (2010).
30. B. E. A. Saleh and M. C. Teich, *Fundamentals of Photonics* (Wiley, 2007).

1. Introduction

Nanophotonic integrated circuits (NPICs) provide a rich toolbox for the investigation of on-chip optical phenomena [1]. Well established lithographic techniques [2] can be used to realize complex waveguide structures from a wide range of materials to confine light and direct it to arbitrary positions along a chip. However, NPICs are typically passive devices that neither allow for the generation nor detection of light and new methods to provide active functionality to NPICs are needed. The monolithic realization of active NPICs in material systems with direct bandgaps such as III-V materials is an obvious route [3], however more flexibility can be achieved by resorting to hybrid integration strategies. These include the use of nanoscale and molecular light sources, which can be positioned on chip through 'pick-and-place' methods with atomic force microscopy [4,5], electron beam lithography and subsequent spin-coating, as well as the direct transfer of 2D materials such as graphene [6,7]. Although these approaches enable on-chip emitters to be positioned in isolated locations more scalable approaches are needed in order to enable the fabrication of emitters arrays in complex nanophotonic circuits. In this regard the use of electrophoretic deposition [8] is particularly attractive as it allows for the deterministic placement of polarizable nanoscale objects such as nanowires [9] and carbon nanotubes [10].

As integrated light sources single-walled nanotubes (SWNTs) are especially attractive because of their tailorable optical properties, which can be selected by control of the diameter or chirality of the nanotube. Furthermore, SWNTs can emit light upon photostimulation [11],

are electroluminescent [12,13] and incandescent [14] and can be used as triggerable photon sources with a small on-chip footprint, as electroluminescent narrow-line [15] or photoluminescent quantum emitters [16]. To date the placement of SWNTs and the coupling of their light emission into planar waveguides [17,18], photonic crystal cavities [19,20] as well as microring resonators [21,22] has been shown. However the integration of SWNT emitters into waveguide structures with directional couplers [23] to enable power splitting has not been shown so far. Here we describe the design and a fabrication method for directional couplers with integrated metallic SWNT-emitters, which can serve as a novel prototypical building block for NPICs and future carbon quantum photonic devices. Single directional couplers are first characterized with externally coupled laser light source and compared to light from on chip SWNT emitter. We are able to show that the splitting ratio determined experimentally with the laser light is reproduced with light from a metallic SWNT emitter. This approach enables a new generation of SWNT-based photon emitters with tailored properties which can be used for optical signal processing within the same circuit.

2. Device design and simulation

In order to enable power splitting on chip, we employed directional couplers consisting of two waveguides with a non-zero overlap of their evanescent fields. We targeted a peak wavelength of 975 nm, which was still within the detection range of a standard silicon CCD camera, whilst also being within the emission spectrum of the SWNT. As a light source we used metallic SWNTs, which provide a broadband thermal emission spectrum with increasing intensity towards infrared wavelengths [14,18].

We chose a rib waveguide geometry with a strip height of 150 nm and a planar layer height of 50 nm beneath it. Both, strip and planar layer consist of a stoichiometric silicon nitride (Si_3N_4) layer. Underneath the structure was a 2000 nm thick layer of buried oxide (SiO_2). The refractive indices are n = 1.98 and n = 1.44, respectively. All waveguides were designed for single mode guidance using finite element method (FEM) simulations (COMSOL Multiphysics). A sweep over the width of the waveguide from 350 nm to 1500 nm shows transverse-electric (TE)-like modes and single-mode characteristic for widths between 350 nm and 800 nm as presented in Fig. 1(a).

After a certain length of the directional coupler, referred to as coupling length (L_c), 100% of the light power is evanescently transferred from the first into the second waveguide. L_c can be conveniently obtained from FEM simulations using the expression [23]

$$L_c = \frac{\lambda}{2 * \left| n_{eff,even} - n_{eff,odd} \right|}.$$ (1)

Here lambda denotes the free-space wavelength of light. The denominator contains the difference of the effective mode indices of the even and odd supermodes, a concept of coupled mode theory (CMT). The mode indices are obtained via COMSOL. Ideally, a directional coupler is designed such that L_c is short to ensure a small footprint but with a waveguide spacing that is suitably large to afford reproducible results after nanofabrication. For a wavelength of λ = 975 nm, L_c was calculated to be 10.3 μm with a feasible gap-size of 250 nm.

We are mostly interested in a 50/50 splitting ratio. The coupling efficiency is proportional to $\sin^2\left(\frac{\pi}{2} * \frac{L_i}{L_C}\right)$ [24]. Therefore for the desired splitting ratio the length of directional couplers (interaction length L_i) should be half of L_c, i.e. 5.15 μm (see Fig. 1(b)).
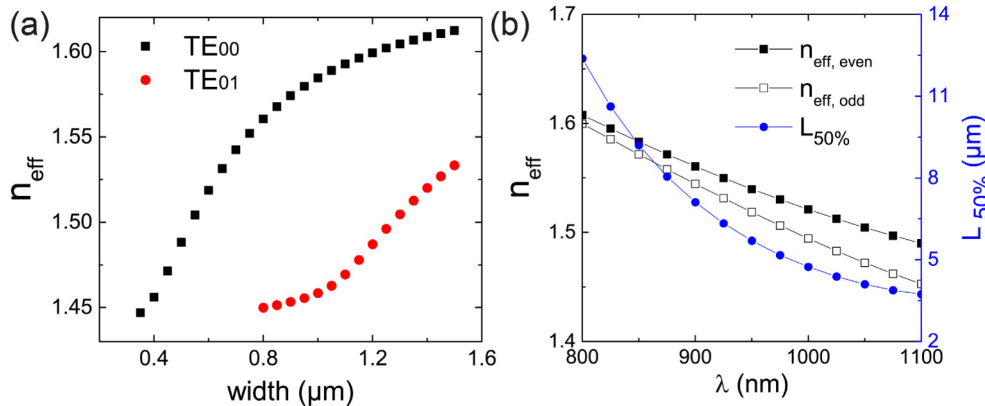
Fig. 1. (a) Relationship between effective refractive indices n_{eff} of guided modes and the waveguide width. n_{eff} is extracted from FEM simulations for TE_{00} and TE_{01} modes. For a width between 375 nm and 800 nm, only a single, well confined TE-like mode is guided. (b) Simulation of n_{eff} for the even and odd supermodes of a directional coupler as well as the 50/50 splitting length $L_{50\%} = 0.5 L_c$ for different wavelengths.

3. Device fabrication and optical characterization

In order to take production tolerances into account and to ensure single-mode guiding, we set the waveguide width to 600 nm in the following. Having numerically determined a suitable geometry for efficient 50/50 splitting in the wavelength range of interest, we experimentally realized several coupling geometries. In order to allow for both on-chip and external optical characterization the directional coupler is equipped with two signal inputs. One input allows for external laser light to propagate inside the device. The other input allows the light from a SWNT emitter to couple into the waveguide and propagate through the device.

Two types of devices with directional couplers were fabricated. Initially in order to characterize the coupling behavior we designed devices without SWNTs as shown in Fig. 2(a). The characterization was performed with an external light laser source which was coupled into and out of a Mach-Zehnder interferometer (MZI) by means of grating couplers (labelled C1, C2, C3). Grating couplers enable the transfer of light into and out of the waveguide from an optical fiber that is brought close to the grating [25]. The light propagating inside the waveguide towards the grating is scattered in a certain angle and captured by the optical fiber above the grating. The MZI consisted of two waveguides split by a directional coupler (DC1) and then recombined (DC2).

The second class of devices contained SWNTs as shown in Fig. 2(c). These devices consisted of four basic elements: waveguide structures, grating couplers, a directional coupler and metal contacts for electrical connection to the SWNT-emitters (E). Additionally, the length of the directional couplers were varied as shown in Figs. 2(d) and 2(e) with L_c of 5 µm and 21 µm.

The photonic devices were defined using several steps of electron beam lithography and reactive ion etching [18]. The first lithography step was used to pattern the waveguide structures. Subsequently, the waveguide structures were etched ¾ into the Si_3N_4 layer. After the second lithography step the Au/Cr contacts were realized using ebeam evaporation and lift-off. Subsequently, metallic small diameter SWNTs from the gel filtration method [26–28] were deposited by ac-dielectrophoresis [29]. A drop of diluted suspension was placed on top of the sample and an ac-signal of 5 V, 3 MHz was applied. Due to the electric field gradient between the 1 µm large gap of the electrodes SWNTs have the preference to deposit mainly in this area and to bridge the waveguide. After 5 minutes the sample was rinsed with water and toluene and the voltage was switched off. To improve the contact adhesion we baked the sample for 1.5 hours at 150 °C in an oven.

All deposited SWNT-contacts were electrically characterized in order to select stable devices for the subsequent optoelectronic measurements. The experiments were performed at room temperature in air without further treatment.

4. Optical transmission measurements using an external light source

Prior to the use of SWNT emitters transmission measurements with an external light source were used to characterize the waveguide coupling behavior. Fine positioning of an optical fiber array with a horizontal spacing of 250 μm was achieved with an XYZ piezoelectric positioning system such that a supercontinuum light source (Leukos SM-30-UV) could be coupled to C3 and a spectrometer (OceanOptics JAZ EL 350) to the output C2. Optimal alignment of the fibers was reached when the transmission at C2 was maximized.
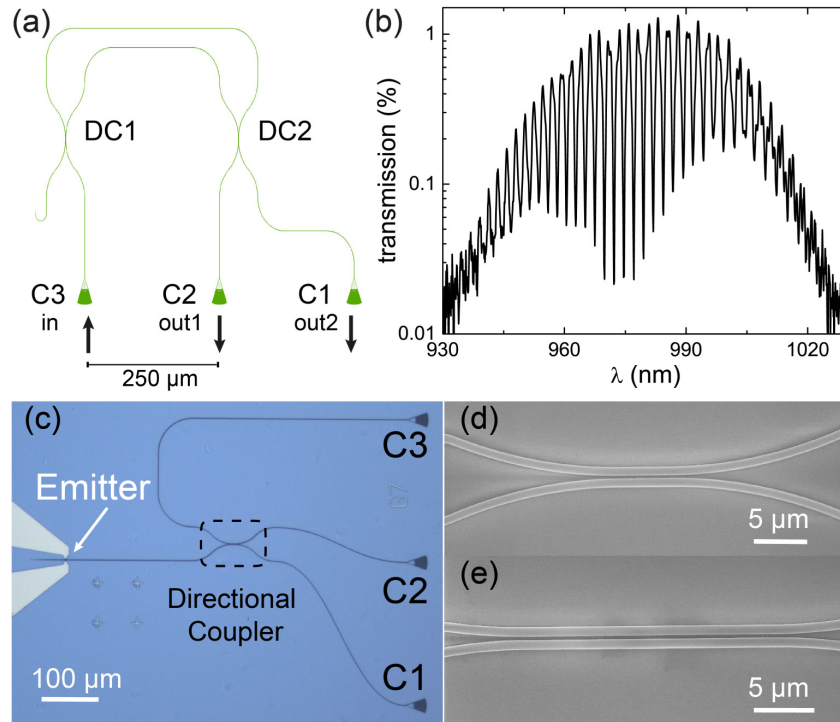

Fig. 2. (a) Schematic layout of a Mach-Zehnder-interferometer (MZI) device for determining the splitting ratio of the directional couplers (DCs). Two directional couplers DC1 and DC2 are used to realize the interferometer with a path length difference of 200 μm. (b) Measured transmission spectrum of MZI device with two DCs with $L_i = 23$ μm. The extinction ratio is the difference between the transmitted intensity maximum and the successive intensity minimum in dB. (c) Optical micrograph of device with electrode pair and two evanescently coupled waveguides with coupler gratings C1, C2, C3. (d,e) Scanning electron micrographs of tilted directional couplers with $L_i = 5$ and 21 μm (all fabricated waveguides are 625 nm wide and 130 nm high). Parameters differ from the parameters used for the simulation due to fabrication imprecisions.

Transmission measurements on devices with an MZI as depicted in Fig. 2(a)) allow for an efficient determination of the optimal parameters of the directional coupler with a 50/50 splitting ratio [30]. The advantage of using a MZI is that it characterizes the coupler devices independent of any losses occurring at the grating coupler. In a MZI the original light beam is split at the first directional coupler (DC1) with a splitting ratio which depends on the wavelength. After a certain path difference both arms of the MZI approach each other at the second directional coupler (DC2). Depending on the phase difference some wavelengths will

interfere constructively while others will interfere destructively, an effect which leads to pronounced fringes in the spectrum as shown in Fig. 2(b). The ratio between a maximum and its subsequent minimum is called the extinction ratio R_e and is defined by

$$R_e = 10 \cdot log_{10} \frac{P_{max}}{P_{min}}. \qquad (2)$$

The higher R_e, the closer is the splitting ratio of the directional coupler to 0.5 for the specific wavelength range.

We realized a series of MZI devices with fixed path length difference of 200 μm (see Fig. 2(a)). The interaction length L_i of both directional couplers in a device is varied around 23 μm and 5.5 μm. R_e was experimentally determined for various different L_i and wavelengths. For each device broadband light from a supercontinuum source was coupled into the device via grating port C1. The transmitted light at both ports C2 and C3 was recorded and analyzed with a spectrometer (Ando AQ-6315). Figures 3(a) and 3(b) show the wavelength dependent R_e for devices fabricated with short and long L_i in the two directional coupler devices. The extinction ratio is color coded. Red implies the highest R_e approaching 17 dB. When the extinction ratio is high the intensity in both MZI arms is well balanced, indicating that the incoming power was evenly split. We observe high reproducibility of results for devices with similar L_i, attesting reliable fabrication. In agreement with our simulations L_i decreases at longer wavelengths (see Figs. 1(b) and Fig. 3). In general, the highest R_e were achieved for devices with L_i being 1-3 μm shorter than it was simulated. The reason for this is the underestimation of L_i in the 2D simulation of the cross section of the directional coupler, because the coupling between both waveguides starts already while they are approaching each other.
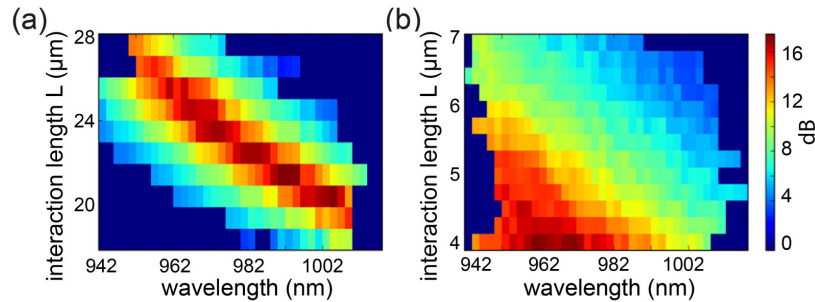

Fig. 3. (a,b) Color-coded measured extinction ratio R_e in dB vs wavelength and L_i. Shown are two measurement series for devices around a coupling length of 23 μm (a) and 5.5 μm (b). R_e is calculated from transmission measurements at port C2. The splitting ratios of the directional couplers are close to 50%, if R_e starts to diverge, thus indicating nearly perfect constructive interference (see Eq. (2). Wavelength regions with high R_e are colored red.

After determining the optimal parameters for 50/50 splitting in the wavelength range of 950-1000 nm by means of MZIs, SWNT-based devices with directional couplers with L_i of 5 μm and 21 μm were fabricated and characterized (see Figs. 2(c) and 2(d)). The spectra were measured in a similar way as described above, except that after the recording of spectra at C2 we consecutively measured the spectrum at C1 as well (Fig. 4). This procedure allows for the calculation of coupling efficiencies.

The transmission spectra of light propagating directly to output C2 and light propagating to output C1 via the directional coupler have a similar Gaussian-shaped envelope due to the influence of the grating couplers. Each coupler provides an insertion loss of roughly 10 dB, leading to an overall transmission through the device of roughly 1%. The crossing of the spectral intensity at 945 nm (black and red curves) and 975 nm (blue and green curves) for shorter and longer L_i indicate the 50/50 splitting point at mentioned wavelengths.

5. Emission measurements using integrated SWNT emitters

Light emission experiments with an electrically driven SWNT emitter were then performed using free-space spectroscopy and a custom imaging setup. This setup has the advantage of not requiring any optical fibers for the coupling of light in or out of the waveguides. Thereby coupling losses and alignment procedures can be avoided and it is possible to conveniently readout low light intensities over a broad wavelength range and to map out spatial intensity distributions.

The measurement setup allows for the emitted light from electrically driven SWNTs to be monitored over a large area with a highly sensitive CCD camera (Princeton Instruments PIXIS 256E Silicon) [18]. Upon passing current through the metallic SWNTs (labeled E in Fig. 5(a)) they start to emit light due to electrical heating. The light efficiently couples into the underlying waveguide and propagates to the directional coupler. Depending on L_i and the wavelength the light partly evanescently couples into the adjacent waveguide and propagates further to the terminating grating couplers C1 and C2. Once the propagating light hits the grating coupler it is scattered into the far field and collected with a microscope objective.
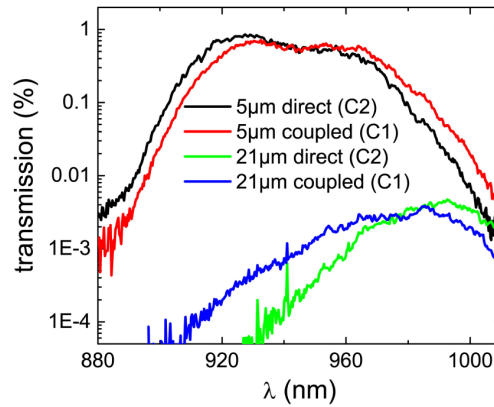

Fig. 4. Transmission spectra of devices with deposited metallic SWNTs as shown in Fig. 2. The transmission was measured between C3 and C2 (black, green) and also between C3 and C1 (red, blue) with an external supercontinuum light source.
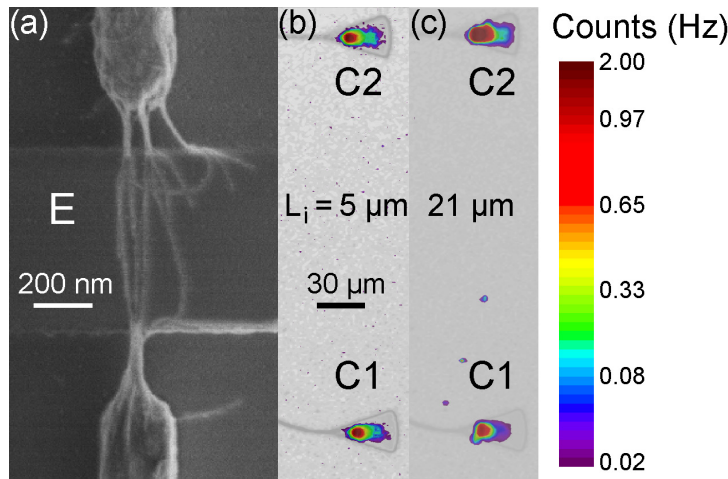

Fig. 5. (a) Scanning electron micrograph of the central part (E) with metallic SWNTs on top of waveguide between two metal contacts. (b,c) High-resolution CCD camera images of the light emission observed on grating couplers C1 and C2; superimposed with grayscale images of the samples with L_i of 5 and 21μm.

The imaging setup allows the light intensity to be simultaneously measured at both grating couplers C1 and C2. For devices with shorter L_i the measured integral intensity of light at both couplers is nearly equal as shown in Fig. 5(b). In case of devices with longer L_i the intensity of directly propagated light measured at C1 is much weaker than the intensity of coupled light measured at C2 (see Fig. 5(c), note the logarithmic color scale). This is in good agreement with the transmission measurements from the previous section where the intensity of the directly propagated light measured at C2 is weaker than the intensity of the coupled light measured at C1 almost for the entire accessible spectral range (Fig. 4).

A detailed analysis of this observation can be provided by spectral measurements at the grating couplers as shown in Fig. 6(a). Here we separate the collected intensity using a spectrometer (Acton SpectraPro 2360). According to the spectra the emission of metallic SWNTs is a black-body radiation with intensity modulation due to the interference with the substrate, as explained in detail in our previous work [18]. The light is collected from a wide solid angle due to the high numerical aperture of the microscope objective. It is therefore not restricted to a certain angle like the fiber array and the measured spectrum does not show the Gaussian profile of the grating coupler. Hence the accessible wavelength range is more than two times broader and the detection of light much more efficient as in transmission.

The measurements in transmission and emission modes allow for extracting the coupling efficiency which is defined as $I_{coupled}/(I_{coupled} + I_{direct})$, where I_{direct} is the intensity of direct propagated light and $I_{coupled}$ is the intensity of coupled light measured at corresponding grating couplers (see Fig. 2(c)). The extracted efficiencies as shown in Fig. 6(b) fit perfectly to each other both for short and long directional couplers. Here we plot the coupling efficiencies extracted both from transmission measurements and from the emission profiles of the SWNT (solid lines). The extraction range of the transmission measurements is limited in spectral range because of the coupling bandwidth of the grating couplers. With both geometries 50/50 splitting ratio is obtained near 975 nm, as predicted from the numerical simulations.
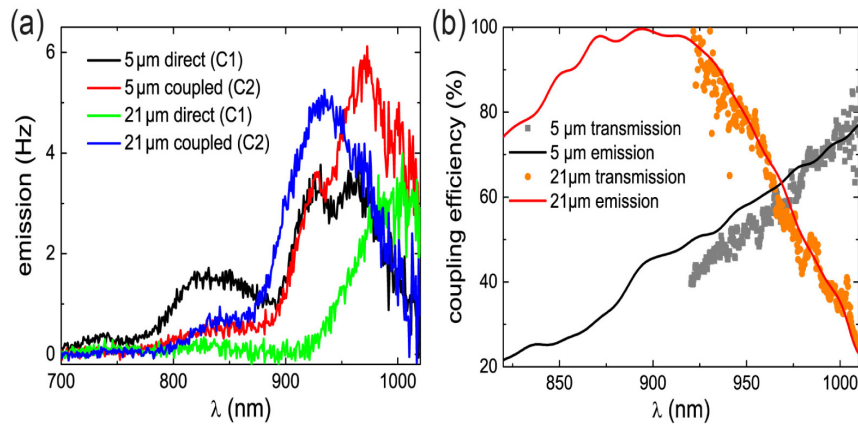

Fig. 6. (a) SWNT-emission spectra simultaneously measured at C1 and C2 for the devices with 5 and 21 µm long L_i (compare with Fig. 4). (b) Coupling efficiency calculated from the data measured for 5 and 21 µm long devices in transmission and emission modes.

The splitting ratio of a directional coupler is a function of its interaction length and the wavelength. An interaction length that leads to a 50/50 splitting ratio for a certain wavelength (in case of the red and black spectra these are L_i = 5 µm and λ = 945 nm) causes a different splitting ratio for shorter and longer wavelengths. Therefore, for λ = 830 nm the interaction length is too short for 50/50 or higher splitting ratios. Hence the direct signal (black) is higher than the coupled signal (red). For λ = 970 nm more than 50% of the light is transferred into the coupled waveguide, leading to an inversion of the signal strengths. For the green and blue curves (interaction length L_i = 21µm) the coupled signal dominates in the spectrum for

wavelengths shorter than the 50/50 splitting ratio wavelength, whereas the direct signal dominates for longer wavelengths. Due to the long interaction length, the light is first completely transferred to the coupled waveguide and then couples back to the direct waveguide. This leads for $\lambda = 975$ nm to a 50/50 splitting ratio because half of the light is coupled back to the direct waveguide.

6. Conclusions

SWNT nanoscale emitters provide a versatile route to lend active functionality to otherwise passive NPICs. Because such emitters can be deterministically aligned to designed metal contacts via electrophoretic deposition, they enable optical analysis of on-chip photonic circuits without the need for fiber input coupling. This way the rich toolbox of nanophotonics can be used to design desired light circuits that process emitted light on-chip. Here we used a directional coupler with a 50/50 splitting ratio for a wavelength of 975 nm for on-chip power splitting as a fundamental building block for future hybrid SWNT-nanophotonic components. The coupling efficiency is measured with a fiber based setup by means of an external light source and with a free-space setup with an integrated SWNT-based source. Both results are highly reproducible and show good fabrication accuracy as a prerequisite for future carbon photonic devices. In particular, this design can also be used in combination with semiconducting SWNTs, thus enabling correlation measurements of the narrow-band emission in the few photon regime.

Acknowledgments